I&EC research
Industrial & Engineering Chemistry Research

Article

pubs.acs.org/IECR

Construction of a Novel Colitoxin DNA Biosensor Based on Cross-Linker-Free Fixation of Probe Fragments on the Interface of Rugby-Ball-Shaped CoS_2 Submicroparticles and Poly(2-thiophenesulfonyl chloride) Composite Film

Xiaoqian Chen, Qingxiang Wang,* Liheng Wang, Hongxu Guo, Yizhen Yang, Feiming Li, and Feng Gao

Department of Chemistry and Environment, Fujian Provincal Key Laboratory of Modern Analytical Science and Separation Technology, Minnan Normal University, Zhangzhou 363000, PR China

ABSTRACT: Rugby-ball-shaped CoS_2 ($rCoS_2$) submicroparticles have been synthesized via a simple hydrothermal reaction. The $rCoS_2$ submicroparticles were then casted on a glassy carbon electrode and served as a highly conductive and large surface area platform for the electrosynthesis of poly(2-thiophenesulfonyl chloride) (pTSC), using 2-thiophenesulfonyl chloride as the monomer. The stepwise modification process was characterized by attenuated total reflectance−Fourier transform infrared spectroscopy (ATR-FTIR) and different electrochemical technologies. The stable pTSC layer was utilized as a functional interface to immobilize amino-modified probe DNA via a facile sulfonyl−amino condensation reaction, without the assistance of any other cross-linkers. Because of the synergistic effect of $rCoS_2$ and pTSC from the hybrid material, the developed DNA biosensor could detect target DNA over a wide dynamic range, from 1.0×10^{-13} to 1.0×10^{-7} M, with the detection limit down to 1.1×10^{-14} M. Benefiting from the steady electropolymerization film of pTSC and the stable sulfamide bond between the amino-modified DNA and pTSC, the biosensor also showed high stability, reusability, and reproducibility.

1. INTRODUCTION

Since the late 20th century, electrochemical DNA biosensors have received great attention in both theoretical and practical aspects because they hold widespread potential application in various fields such as food safety and quality,[1,2] drug screening,[3] environment monitoring,[4] clinical diagnosis,[5,6] etc. Although some new strategies such as nanoparticle labeling,[7] molecule beacons,[8] and enzyme-assisted target recycling[9] have been introduced into the fabrication of the high-powered DNA biosensors, the fixation of the probe DNA on the transducer surface is still a basic and critical step because it has great impact on the performance of DNA biosensors including the sensitivity and efficiency as well as the stability, regeneration ability, and reproducibility.

To improve the performance mentioned above, inorganic semiconductive materials with submicro- or nanosize provide a popular solution because of their large surface area, good biocompatibility, high catalytic capacity, and excellent chemical and physical stability.[10−12] However, the application of single-part inorganic particles is limited in biosensor fabrication because they usually have poor adhesion to the basal surface and lack the organic functional groups to tightly graft with the probe biomolecules. Therefore, the stability and regeneration of the biosensor produced by this approach is hard to guarantee. To circumvent such problems, incorporation of organic polymers into the inorganic particles via chemical assembly or physical doping to form hybrid functional materials received much attention because they not only maintain the intrinsic high-conductivity, large surface area, and strong mechanics of the inorganic components, but also exhibit the functionality and chemical homogeneity of the organic portion.[11−13]

In this work, a novel hybrid material containing rugby-ball-shaped cobalt sulfides ($rCoS_2$) submicroparticles and poly(2-thiophenesulfonyl chloride) (pTSC) was modified on a glassy carbon electrode (GCE) and used as the functional platform for biological probe (DNA) immobilization. Cobalt sulfide is a type of important II−IV semiconductive material with wide application in catalysts, capacitors, lithium battery cathodes, scanning probes, and photoconductor materials because of its unique catalytic, electrical, and magnetic properties.[14,15] However, its application in the construction electrochemical biosensors has been scarcely reported. On the other hand, the material of polythiophene, an environmentally and thermally stable conjugated polymer, has been widely used in chemical sensors,[16,17] light-emitting diodes,[18] photovoltaic deviced,[19] and transistors[20] because of its versatile synthetic approaches, easy functionalization, and unique electronic properties. The high electrical conductivity resulting from the delocalization of electrons along the polymer backbone also indicate great promise in the application of electrochemical sensors.[21,22] Electrochemical polymerization is a convenient approach for preparing polythiophene, through which the product can be easily isolated and purified.[23,24] To enlarge the application of polythiophene in biosensors, much effort has been carried out in recent years to fabricate functionalized polythiophene derivatives through modifying the thiophene monomer with the functional groups.[25−27] Inspired by this research, the thiophene derivative of 2-thiophenesulfonyl chloride was

Received: May 21, 2014
Revised: December 20, 2014
Accepted: January 15, 2015
Published: January 15, 2015

DOI: 10.1021/ie503831k
Ind. Eng. Chem. Res. 2015, 54, 1520−1528

chosen as the monomer for the electrosynthesis of polythiophene in this work, through which not only the stable and uniform thiophene polymer film was synthesized on the electrode surface, but also the highly active functional group of sulfonyl was introduced.

The experimental results showed that the hybrid film of $rCoS_2$/pTSC could be facilely prepared. In addition, the amino-modified probe DNA can be easily grafted on the surface of $rCoS_2$/pTSC via the one-step sulfonyl−amino condensation reaction. This approach does not require the aid of any cross-linkers, such as 1-ethyl-3-(3-(dimethylamino)propyl)-carbodiimide (EDC), ethylenediamine, or glutaraldehyde, which are often used for bioconjugation assays. The obtained biosensor displays good stability and regenerability because of the beneficial effects of electropolymerization and covalent immobilization of probe DNA. Moreover, because of the large accessible area and high electrocatalysis of the $rCoS_2$ component in the hybrid film, the DNA biosensor shows high electrochemical response in hybridization detection. When the DNA fragments from the colitoxin was used as a model for analysis, the target DNA could be detected down to 1.1×10^{-14} M, which suggested that the strategy developed in this work opens a facile and low-cost approach for colitoxin detection in clinical diagnosis, environment monitoring, and food analysis.

2. EXPERIMENTAL PROCEDURE

2.1. Chemicals. Thiourea, cobalt nitrate hexahydrate ($Co(NO_3)_2{\cdot}6H_2O$), and sodium perchlorate ($NaClO_4$) were provided by Aladdin Reagent (China). TSC was supplied by Meryer Chemical Reagent (China). *N*,*N*-dimethylformamide (DMF), ethylenediaminetetraacetic acid (EDTA), tris (hydroxymethyl) aminomethane (Tris), and ethylene glycol were obtained from Xilong Chemical Reagent (China). Methylene blue (MB) was obtained from Shanghai Chemical Reagent (China). All the other chemicals were of analytical reagent grade and used without further purification. Phosphate buffer saline (PBS) was prepared by mixing 20 mM NaCl and 25 mM NaH_2PO_4−Na_2HPO_4. Doubly distilled water (DDW) was used in all experiments.

The 24-base synthetic DNA fragments related to colitoxin[28] were provided by Shanghai Sangon Bioengineering Limited Company (China), with the following base sequences:

- Probe sequence (S1): 5′-NH_2-$(CH_2)_6$-GAG CGG CGC AAC ATT TCA GGT CGA-3′
- Complementary sequence (S2): 5′-TCG ACC TGA AAT GTT GCG CCG CTC-3′
- Single-mismatched sequence (S3): 5′-TCG ACC TGA AAT GTT GCG CC***T*** CTC-3′
- Three-base mismatched sequence (S4): 5′-TCG ***T***CC TGA AA***C*** GTT GCG CC***T*** CTC-3′
- Noncomplementary sequence (S5): 5′-GCA CGG CGC AAC ATT TCA GGT CGA-3′

All the oligonucleotides stock solutions (10 μM) were prepared in TE solution (10 μM Tris−HCl, 1.0 mM EDTA, pH 8.0) and kept frozen.

2.2. Apparatus. The morphology of CoS_2 was characterized by Hitachi model S-4800 scanning electron microscopy (SEM; Japan), Jeol JEM-1230 transmission electron microscopy (TEM; Japan), and Bruker D8-Advance X-ray diffraction (XRD; Germany) instruments. Atomic force microscopy (AFM) characterization for the electrode modification process was carried out on a CSPM-5500 scanning probe microscope (China). Attenuated total reflectance−Fourier transform infrared spectroscopy (ATR-FTIR) was recorded on a NICOLET iS10 IR optical spectrometer (United States). Electrochemical measurements were carried out on a CHI 650D electrochemical analyzer (China) with the conventional three electrode system: a glassy carbon electrode (GCE; Φ = 2 mm) modified with different materials was used as working electrode, Ag/AgCl as reference electrode, and platinum wire as auxiliary electrode.

2.3. Preparation of the $rCoS_2$. The rugby-ball-shaped cobalt sulfides were synthesized by a facile hydrothermal reaction. In a typical procedure, 2.4 mmol of thiourea, 0.8 mmol of $Co(NO_3)_2{\cdot}6H_2O$, and 1.0 mL of polyethylene glycol were successively added to 120 mL of ethylene glycol. The mixture was stirred for 30 min under room temperature. Then, the resulting homogeneous solution was transferred into a 150 mL stainless steel autoclave up to about 80% of its capacity, kept at 180 °C for 12 h, then cooled to room temperature naturally. The precipitates were washed with DDW and ethanol several times. Thereafter, the sample was dried at 100 °C for 2 h in a vacuum.

2.4. Preparation of the pTSC/$rCoS_2$/GCE. First, 1.0 mg of $rCoS_2$ was dispersed in 1 mL of DDW and sonicated for 30 min to obtain uniformly dispersed 1.0 g L^{-1} $rCoS_2$ solution. Then, the GCE was carefully polished to a mirror-like surface with 0.3 and 0.05 μm alumina slurries, followed by ultrasonication in anhydrous ethanol and DDW for 5 min each. After the electrode was dried under N_2 stream, 10 μL of 1.0 g L^{-1} $rCoS_2$ dispersion was cast on the cleaned GCE surface and dried in air. Then, the modified electrode was immersed into 0.05 M TSC solution containing 0.01 M $NaClO_4$ for electropolymerization, which was performed through cyclic scanning in the potential range from 0 V to +1.4 V for 10 cycles with a scan rate of 10 mV s^{-1}. Before the scanning, the TSC solution was purged with N_2 for 20 min to remove the oxygen, and the whole electropolymerization process was under the protection of N_2 atmosphere. The as-prepared electrode was then washed three times with $NaClO_4$ and DDW separately to remove the unpolymerized TSC monomer; thus, the poly(2-thiophene-sulfonyl chloride) modified electrode (pTSC/$rCoS_2$/GCE) was obtained.

2.5. Probe DNA Immobilization and Hybridization. The DNA probe was immobilized on pTSC/$rCoS_2$/GCE through a facile and direct sulfonyl−amino condensation reaction. Briefly, the preprepared electrode of pTSC/$rCoS_2$/GCE was immersed into 1.0 mL of TE buffer solution containing 1.0×10^{-7} M S1 at room temperature for 12 h and then rinsed with TE buffer to eliminate the physically absorbed DNA. Thus, an S1-modified electrode (S1/pTSC/$rCoS_2$/GCE) was obtained. For the hybridization process, the S1/pTSC/$rCoS_2$GCE was incubated in TE buffer solution with desired concentration S2 for 45 min at 42 °C. After the hybridization reaction, the electrode was washed with TE buffer to eliminated the unhybridized DNA. The hybridized electrode is denoted as S2−S1/pTSC/$rCoS_2$/GCE. The hybridizations of the probe DNA with the single mismatched DNA (S3), the three-base mismatched DNA (S4), and the noncomplementary DNA (S5) were performed through a similar procedure, and the obtained electrodes are termed S3−S1/pTSC/$rCoS_2$/GCE, S4−S1/pTSC/$rCoS_2$/GCE, and S5−S1/pTSC/$rCoS_2$/GCE, respectively.

2.6. Voltammetric Detection. Electrochemical impedance spectroscopy (EIS) was applied to characterize the modification

DOI: 10.1021/ie503831k
Ind. Eng. Chem. Res. 2015, 54, 1520−1528

Scheme 1. Fabrication and Detection Procedures of the DNA Biosensor Using pTSC-rCoS$_2$ as the Probe DNA Immobilization Platform

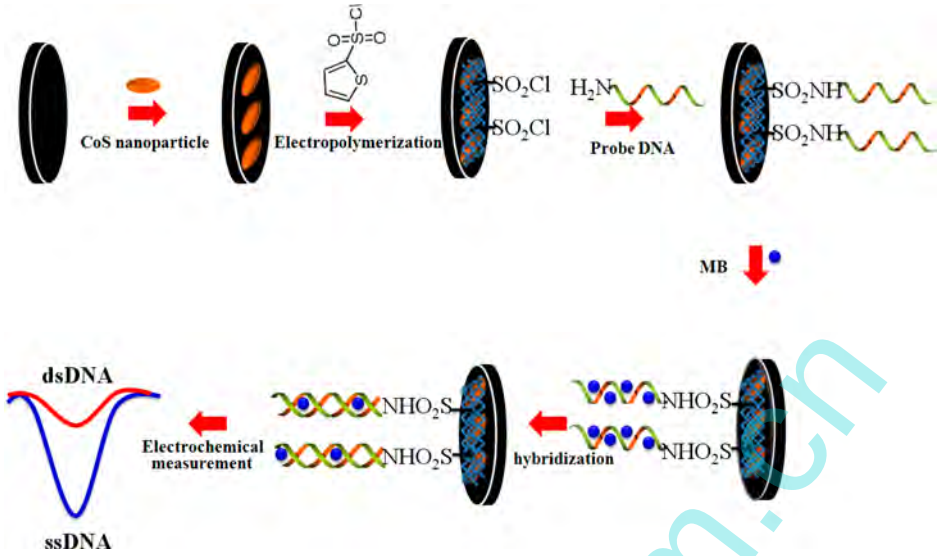

process of the biosensor, which was measured in 1.0 mM $[Fe(CN)_6]^{3-/4-}$ prepared in 0.1 M KCl and collected at a potential of +0.192 V in the frequency range from 0.5 to 10 kHz with the voltage amplitude of 5 mV. The hybridization detection of the DNA biosensor was accomplished using MB as the redox indicator with the following procedures: first, the S1/pTSC/rCoS$_2$/GCE was immersed into 25 mM PBS buffer solution containing 10 μM MB for 20 min under open circuit to sufficiently bind MB molecules. Then the electrode with the adsorbed MB was washed with PBS buffer solution for 30 s, followed by electrochemical detection in a blank PBS buffer solution with differential pulse voltammetry (DPV) between −0.5 and 0 V, including a potential increment of 0.004 V, pulse amplitude of 0.05 V, pulse width of 0.05 s, and pulse period of 2 s. The detailed construction and detecting procedures for the developed DNA biosensor are illustrated in Scheme 1.

3. RESULTS AND DISCUSSION

3.1. Morphology and Structure Characterization of rCoS$_2$. The phase and morphology analysis of the as-prepared rCoS$_2$ were investigated by XRD, SEM, and TEM. Figure 1A shows the typical XRD pattern of the synthesized rCoS$_2$ particles, in which the main diffraction peaks could be assigned to a cubic phase of CoS$_2$ (JCPDS entry 65-3322), indicating that pure and highly crystalline CoS$_2$ was obtained. Panels B and C of Figure 1 show the low- and high-magnification SEM images of the prepared rCoS$_2$, respectively. In the low-magnification SEM image, it can be found that large amounts of particles were observed, demosnstrating high yield of the synthesized CoS$_2$ products. The high-magnification image further demonstrates that single CoS$_2$ particles show a rugby-ball shape. The transverse and longitudinal diameters of the rugby-ball structure were estimated to be 1.1−1.3 μm and 0.8−0.9 μm, respectively, suggesting the submicrostructure of the synthesized sample. The TEM image displayed in Figure 1D further indicates that the synthesized CoS$_2$ had the unique rugby-ball shape. In addition, from the SEM and TEM images, it can be observed that the rCoS$_2$ particles had coarse and loose structure on their surface, suggesting the large surface area characteristic of the as-synthesized sample.

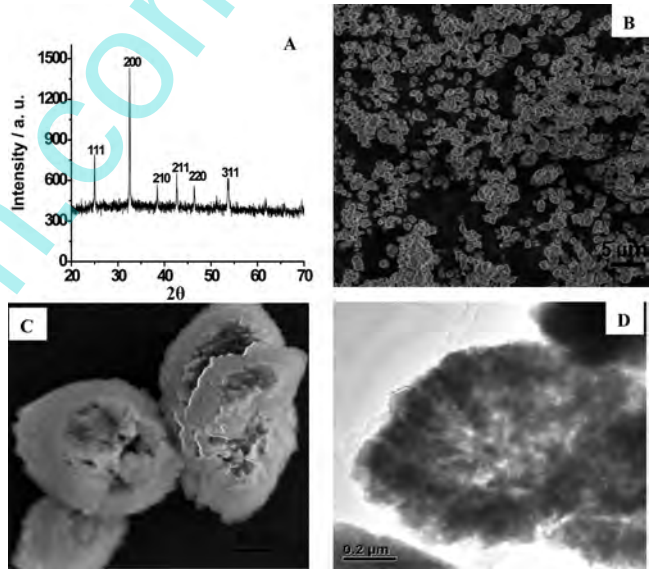

Figure 1. Typical XRD pattern (A), low-magnification (B) and high-magnification (C) SEM images, and TEM image (D) of the as-synthesized rCoS$_2$.

3.2. Characterization on the Biosensor Fabrication. Atomic force microscope is a high-resolution scanning probe microscopy, which can provide the microscopic and three-dimensional (3D) morphology of a surface. Figure 2 shows the topographic (a), cross-sectional graph (b), and 3D (c) AFM images of bare GCE before (A) and after stepwise modification of rCoS$_2$ (B) and pTSC (C). It can be seen that the bare GCE showed a relatively flat and smooth surface with the largest height of 4.57 nm. The average roughness (R_a) value calculated from different regions was 2.68 nm, which was consistent with the value of a bare GCE reported in the literature.[29] When rCoS$_2$ was cast on the electrode surface, the morphology changed obviously, and it was observed that some particles were distributed on the electrode surface. The larget peak height and the average roughness were increased to 246.90 and 16.9 nm, respectively, suggesting that the rCoS$_2$ submicroparticals had been cast on the bare GCE. After electropolymeriza-

DOI: 10.1021/ie503831k
Ind. Eng. Chem. Res. 2015, 54, 1520−1528

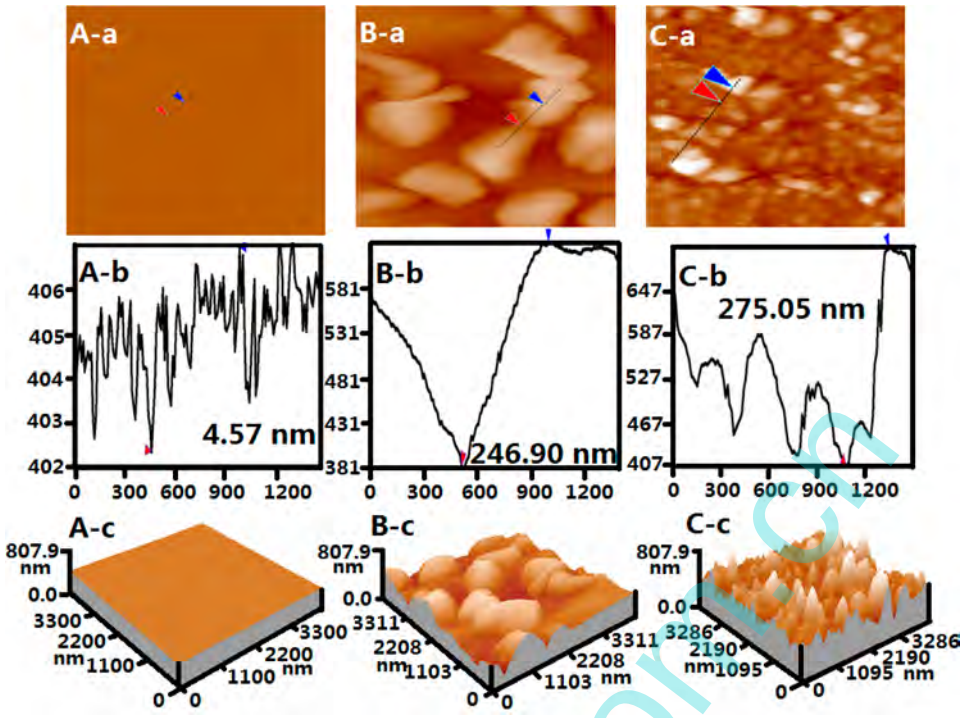

Figure 2. AFM images of bare GCE (A), $rCoS_2$/GCE (B), and pTSC/$rCoS_2$/GCE (C).

tion of TSC on $rCoS_2$/GCE, some uniform and adjacent forestlike peaks appeared, and meanwhile the height and the average roughness were further increased to 275.05 and 24.7 nm, respectively. This result demonstrated that poly-TSC film had been modified on the surface of $rCoS_2$/GCE through the electrochemical method.

The stepwise modification of $rCoS_2$ and pTSC on the electrode surface was further examined by ATR-FTIR, and the results are depicted in Figure 3. As can be seen, the bare GCE

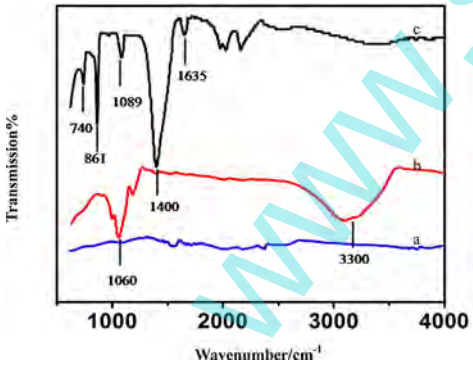

Figure 3. ATR-FTIR spectra of bare GCE (a), $rCoS_2$/GCE (b), and pTSC/$rCoS_2$/GCE (c).

did not produce any significant feature in the spectra (curve a). However, on $rCoS_2$/GCE, a strong peak at 1060 cm^{-1} attributable to Co═S stretching in the presence of CoS_2 was observed (curve b).[30] Additionally, a broad absorption band appeared at 3300 cm^{-1}, which could be ascribed to the O−H stretching vibration of the residual solvent molecules. When the pTSC layer was electrochemically synthesized on $rCoS_2$/GCE, the characteristic peak observed on $rCoS_2$/GCE disappeared completely (curve c), showing that the $rCoS_2$ had been covered. The newly emerged strong absorption band at 1400 cm^{-1} could be assigned to the absorption of $-SO_2Cl$.[31] The peak presented at around 1635 cm^{-1} was related to the symmetric stretching vibration of C═C on the thiophene ring. The absorption peaks at 740 and 861 cm^{-1} were due to the bending vibration of C−H of the thiophene ring.[32] These changes indicate that the polymer film of pTSC had been electrodeposited on the electrode surface.

EIS is a convenient and sensitive tool for probing the interface properties of the modified electrodes.[33] Figure 4 illustrates the typical Nyquist diagrams obtained on different modified electrodes in 1.0 mM $[Fe(CN)_6]^{3-/4-}$ prepared in 0.1 M KCl and the corresponding electrical equivalent circuit (inset). In this circuit, the parameter R_s represents the solution resistance and R_{ct} is the charge-transfer resistance, which

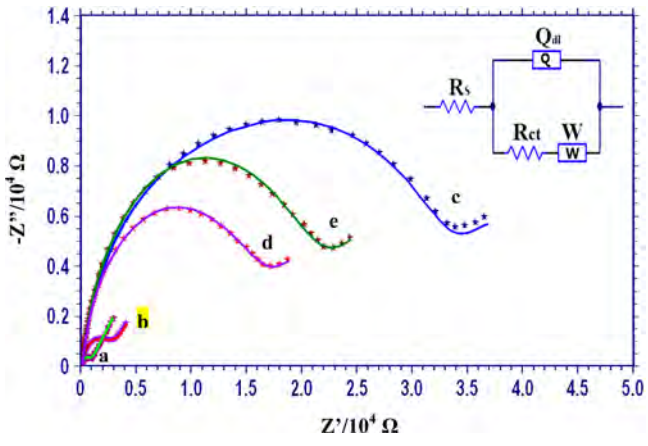

Figure 4. Nyquist plots (Z_{im} vs Z_{re}) for the Faradaic impedance measurements of 1.0 mM $[Fe(CN)_6]^{3-/4-}$ prepared in 0.1 M KCl at (a) bare GCE, (b) $rCoS_2$/GCE, (c) pTSC/GCE, (d) pTSC/$rCoS_2$/GCE, and (e) S1/pTSC/$rCoS_2$/GCE. Inset shows the equivalent circuit model used for impedance data analysis.

DOI: 10.1021/ie503831k
Ind. Eng. Chem. Res. 2015, 54, 1520−1528

Table 1. Simulated Values of the Equivalent Circuit Elements for the Different Modified Electrodes

electrode	R_s (Ω cm^2)	Q_{dl} (μF cm^{-2})	n	R_{ct} (Ω cm^2)	W (mΩ cm^2)
GCE	9.337	34.11	0.8812	49.34	3.835
$rCoS_2$/GCE	9.721	14.34	0.8032	189.4	0.502
pTSC/GCE	10.31	16.76	0.8617	1596	0.561
pTSC/$rCoS_2$/GCE	9.760	26.35	0.8909	1094	1.904
S1/pTSC/$rCoS_2$/GCE	9.283	17.31	0.8971	1437	1.568

reflects the counterion transfer happening at the film−electrolyte interface. The diffusion of the counterions through the modified film is described by Warburg element, W, and the element Q_{dl} is the double-layer capacitance. Among these elements, the R_{ct} is the most direct and sensitive parameter to demonstrate the electron-transfer kinetics of the redox probe on the electrode surfae.[34] The fitting results (solid lines) show that the equivalent circuit model has a good agreement with the real experimental data (dotted curves), and the obtained parameters are summarized in Table 1. From the result, he R_s component in terms of the solution resistance remained constant at 9.28−10.3 Ω cm^2, as would be expected for measurements under identical conditions of supporting electrolyte concentration and temperature. In addition, the relatively small R_{ct} values of 49.34 Ω cm^2 and 189.4 Ω cm^2 were observed for bare GCE (curve a) and $rCoS_2$/GCE (curve b), respectively. However, when the GCE was directly electrodeposited with TSC, the R_{ct} value was sharply increased to 1596 Ω cm^2 (curve c), suggesting that the single-component film of pTSC inhibited the electron-transfer process on the electrode surface by its inferior conductivity. Interestingly, when TSC was electropolymerized on GCE that had been precoated with $rCoS_2$ (i.e., $rCoS_2$/GCE), the R_{ct} value was significantly decreased to 1094 Ω cm^2 (curve d), indicating that the $rCoS_2$ submicropartcles provided highly conductive charge pathways between the electrode and the electrolyte. Furthermore, after the pTSC/$rCoS_2$/GCE was incubated in S1 solution for probe DNA grafting, the R_{ct} value increased again (1437 Ω cm^2, curve e), suggesting that the probe DNA had been successfully immobilized on the electrode surface, and electron transfer was blocked by the electrostatic repulsion between the negatively charged probe DNA and $[Fe(CN)_6]^{3-/4-}$ anions. These results also indicated that a novel DNA biosensor could be fabricated through one-step bioconjuction between sulfonyl group on pTSC film and modified amino group on probe DNA. Compared with the other DNA immobilization methods based on amino−carboxyl,[35] sulfonic−amino,[36] or amino−aldehyde condensations,[37] neither preactivating reagents, such as 1-ethyl-3-(3-dimethyl aminopropyl) carbodiimide (EDC), *N*-hydroxysuccinimide (NHS), and phosphorus chloride (PCl_5), nor cross-linkers like glutaraldehyde was needed, suggesting that the method presented in this work was more convenient and inexpensive.

3.3. Effect of $rCoS_2$ on the Electrochemical Performance of the Biosensor. To further investigate the effect of $rCoS_2$ on the electrochemical performance of the biosensor as a novel electrode material, the effective surface area (A) and electron-transfer rate constant (K_s) of the electroactive molecules at the modified electrodes with $rCoS_2$ were investigated. Figure 5A shows the chronocoulometric (CC) plots of pTSC/GCE (a) and pTSC/$rCoS_2$/GCE (b) in 1.0 mM $[Fe(CN)_6]^{3-/4-}$ prepared in 0.1 M KCl. According to the Anson equation[38]

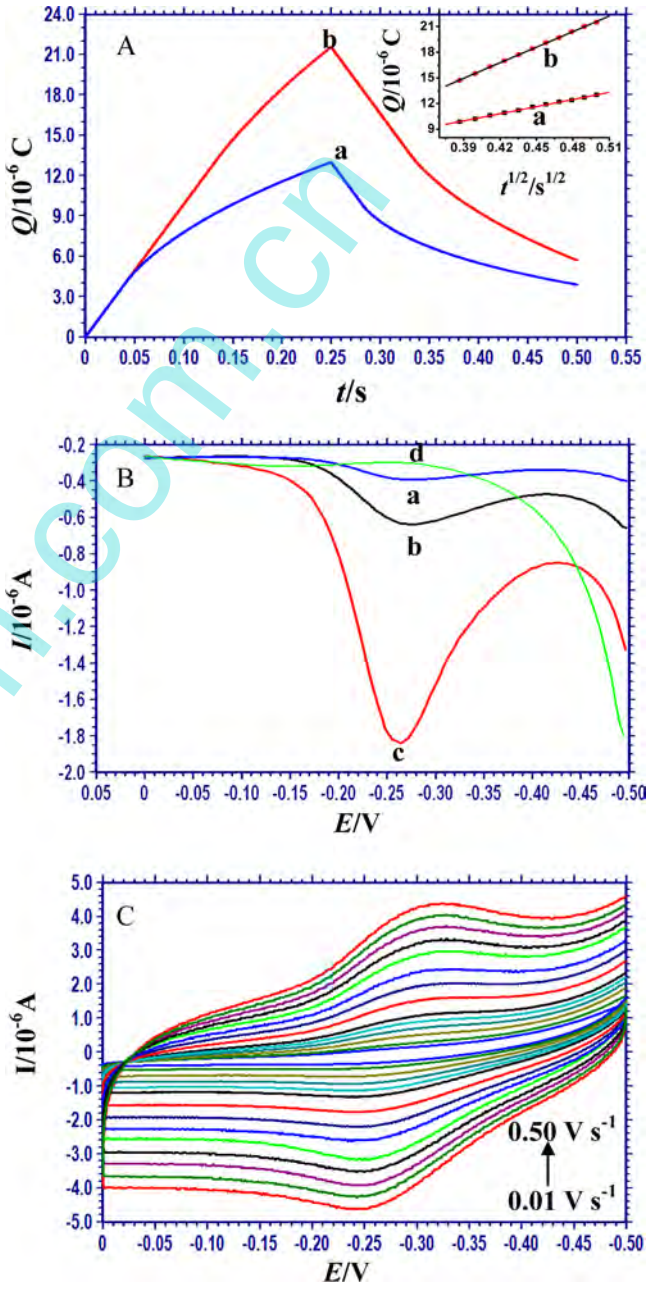

Figure 5. (A) Chronocoulometric curves of pTSC/GCE (a) and pTSC/$rCoS_2$/GCE (b) in 1.0 mM $[Fe(CN)_6]^{3-/4-}$ prepared in 0.1 M KCl and the corresponding plots of Q versus $t^{1/2}$. (B) DPVs of (a) pTSC/$rCoS_2$/GCE, (b) S1/pTSC/GCE, and (c) S1/pTSC/$rCoS_2$/GCE in blank PBS solution after the electrode incubation in 1.0 × 10^{-5} M MB for 25 min. Curve d is the DPV of S1/pTSC/$rCoS_2$/GCE in PBS solution without preaccumulation in MB solution. (C) Dependence of CVs of MB at S1/pTSC/$rCoS_2$/GCE on scan rate (ν) in blank PBS solution. From inner to outer: 0.01, 0.02, 0.04, 0.06, 0.08, 0.10, 0.15, 0.20, 0.25, 0.30, 0.35, 0.40, 0.45, and 0.50 V s^{-1}.

DOI: 10.1021/ie503831k
Ind. Eng. Chem. Res. 2015, 54, 1520−1528

$$Q = Q_{dl} + Q_{ads} + 2nFAC(Dt/\pi)^{1/2}$$

where Q_{dl} is the double layer charge, which can be eliminated by background subtraction; Q_{ads} the Faradaic charge; n the number of transferred electrons; F the Faraday constant; C the concentration of electrolytes; and D the diffusion coefficient. The values of A were determined to be 0.09 and 0.20 cm^2 for pTSC/GCE and pTSC/$rCoS_2$/GCE, respectively. This result suggested that when the submicrosized $rCoS_2$ was modified on the electrode surface, the effective surface area of the electrode could be greatly improved, which is very advantageous for an interface to enhance the immobilization amount of the probe biomolecules.

Additionally, to probe the effect of $rCoS_2$ on the electron-transfer kinetics of the electrode interface, the electrochemical behaviors of a classical electroactive phenothiazine dye (MB) at different electrodes were investigated. Figure 5B shows the DPVs of MB on pTSC/$rCoS_2$/GCE (curve a), S1/pTSC/GCE (curve b), and S1/pTSC/$rCoS_2$/GCE (curve c) in blank PBS buffer solution after the electrodes were incubated in 1.0×10^{-5} M MB for binding equilibrium and then rinsed with PBS. Clearly, only a very weak electrochemical response was observed on pTSC/$rCoS_2$/GCE (curve a), which suggested that pTSC/$rCoS_2$/GCE had negligible nonspecific interaction with the MB molecules. However, on S1/pTSC/$rCoS_2$/GCE (curve c), a well-defined oxidation peak appeared. The peak potential of −0.26 V was very close to the previously reported oxidation potential of MB bound at DNA-modified electrode,[39,40] suggesting that MB had been adsorbed at the electrode surface by the specific interaction of MB with the guanine bases of probe DNA.[41] This conclusion could be further supported by the result that the S1/pTSC/$rCoS_2$/GCE without preaccumulation in MB did not display any electrochemical signal in blank PBS solution, as displayed in curve d. Moreover, it was found that the electrochemistry of MB on S1/pTSC/GCE (curve b) was far less than that on S1/pTSC/$rCoS_2$/GCE, proving that the presence of $rCoS_2$ in the modified film significantly enhanced the electrochemical response of the biosensor.

Figure 5C shows the influence of scan rate (v) on the redox peak current of MB at S1/pTSC/$rCoS_2$/GCE. It was observed that both reduction peak currents (I_{pc}) and oxidation peak currents (I_{pa}) increased gradually with the increase of scan rate, and showed good linearity with the scan rate in the range from 0.04 to 0.50 V s^{-1}, with the linear regression equations of I_{pc} (10^{-6} A) = 0.2677 + 0.0084 v (V s^{-1}) (r = 0.999) and I_{pa} (10^{-6} A) = −0.41477−0.0086 v (V s^{-1}) (r = 0.999). This further revealed that the redox indicator of MB had been bound to S1/pTSC/$rCoS_2$/GCE. On the other hand, with the increase of scan rate, the peak-to-peak separation (ΔE_p) also increased gradually without the change of the formal potential, which was the typical quasi-reversible process. Thus, according to the following Laviron's equations[42]

$$E_{pa} = E^{0'} + \frac{RT}{(1-a)nF}\ln v$$

$$E_{pc} = E^{0'} + \frac{RT}{anF}\ln v$$

$$\log k_s = a\log(1-a) + (1-a)\log a - \log\frac{RT}{nFv} - \frac{nF\Delta E_p a(1-a)}{2.3RT}$$

where a is the electron-transfer coefficient, $E^{0'}$ the formal potential, R the gas constant, T the temperature, and F the Faraday constant. The values of a and k_s of MB at S1/pTSC/$rCoS_2$/GCE were estimated as 0.64 and 6.9 s^{-1}, respectively. For comparison, the values of a and k_s of MB at S1/pTSC/GCE were also determined through the same method (data not shown), and the results were 0.53 and 1.1 s^{-1}, respectively. Obviously, the value of k_s of MB at S1/pTSC/$rCoS_2$/GCE was increased by about 6-fold as compared with that of S1/pTSC/GCE, which experimentally proved that the $rCoS_2$ at the electrode surface had significant signal amplification effect toward the electroactive molecules.

3.4. Analytical Performance of the Biosensor. In this work, the electroactive dye of MB was further used as a redox indicator to monitor the hybridization performance of the developed biosensor. It has been reported that MB could specifically interact with the free guanines of the unpaired single-stranded DNA[41] and present a large electrochemical signal at the probe DNA modified electrode. After the probe electrode was hybridized with the target DNA, the duplex structure was formed between the two complementary strands via the base-paring principle, through which the MB molecules adsorbed on probe DNA would be released from the electrode surface. Thus, by probing the variation of the electrochemical signal of MB, the hybridization event could be monitored.[43−45] The base-mismatch (mutation) of DNA is a very common phenomenon in biological hereditary process, which can induce disease and even death of the cells or organisms. Therefore, the accurate analysis and detection of base-mismatched DNA are of great significance in clinical diagnosis and biological mechanism research. In this work, to probe the hybridization selectivity of the developed biosensor, four kinds of DNA segments including complementary, noncomplementary, single mismatched, and three-base mismatched DNA were chosen as the analytes for analysis using MB as the indicator. Figure 6 shows the DPV signals of MB on S1/pTSC/$rCoS_2$/GCE before and after hybridization with the above-mentioned four different oligonucleotide fragments. The corresponding peak current values on different electrodes are depicted in the histogram in the inset. A large DPV peak was observed at S1/pTSC/$rCoS_2$/GCE because of the specific interaction of MB with guanine residues of S1 (curve a). After the biosensor was hybridized with the complementary sequence of S2, the DPV signal decreased significantly (curve b), suggesting that the double-helix DNA formed on the electrode and the MB molecules were liberated from the electrode surface by hybridization event. When the noncomplementary sequence (S5) was hybridized (curve e), the DPV signal changed negligibly as compared with that of probe DNA modified electrode, which indicated that the hybridization reaction did not happen because of the complete mismatch. The selectivity of the biosensor was also investigated by hybridization with the single mismatched sequence and the three-base mismatched sequence. It was found that the electrochemical signals of MB on these two hybridized electrodes fell between those of S1/pTSC/$rCoS_2$/GCE and S2−S1/pTSC/$rCoS_2$/GCE, showing that only partial hybridization was accomplished for these two

DOI: 10.1021/ie503831k
Ind. Eng. Chem. Res. 2015, 54, 1520−1528

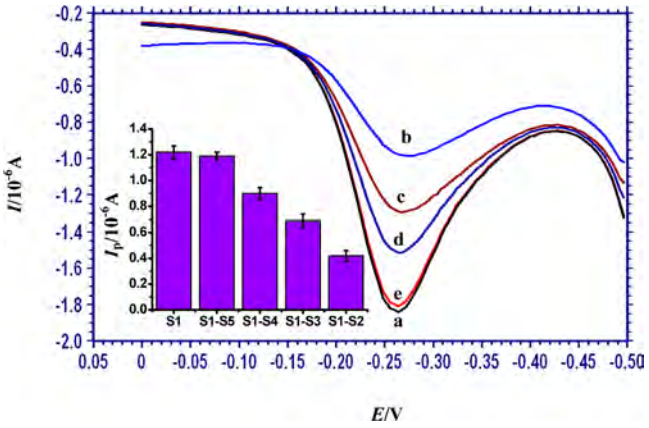

Figure 6. DPVs of MB absorbed on S1/pTSC/$rCoS_2$/GCE before (a) and after hybridization with complementary sequences of S2 (b), single mismatched sequences of S3 (c), three-base mismatched sequences of S4 (d), and noncomplementary sequences of S5 (e) in 25 mM PBS (pH 7.0). The concentrations of all the hybridized sequences are 0.1 μM. Inset shows the corresponding histogram of the peak current values on different electrodes.

sequences. Meanwhile, the peak current on S4−S1/pTSC/$rCoS_2$/GCE was higher than on S3−S1/pTSC/$rCoS_2$/GCE, indicating that the biosensor can also distinguish the target DNA with different mismatching degrees.

The sensitivity of the DNA biosensor was investigated by varying the concentration of the complementary DNA (S2) for hybridization. Figure 7A shows the DPVs of MB on S1/pTSC/$rCoS_2$/GCE before and after hybridization with different concentrations of complementary sequences. Clearly, as the concentration of S2 was increased, the oxidation peak current of MB decreased gradually, which suggested that increasing amount of DNA duplex at the electrode surface was formed through the hybridization reaction. The average peak currents (I_p) of MB showed a linear relationship with the negative logarithmic values of the S2 concentrations (−log C_{S2}) ranging from 1.0×10^{-13} to 1.0×10^{-7} M, with the regression equation of I_p (10^{-6} A) = 0.13 log C_{S2} (M)−0.61 and the regression coefficient (r) of 0.9939 (inset in Figure 7A), showing that the target DNA could be detected by the developed biosensor in a wide concentration range. On the basis of 3σ (where σ is the standard deviation of the blank solution, n = 7), the detection limit of the biosensor was estimated to be 1.1×10^{-14} M. Also, the analytical performance of S1/pTSC/GCE to the target DNA was also evaluated, and the DPVs of MB on S1/pTSC/GCE upon hybridization with increasing amount of S2 are displayed in Figure 7B. From the result, the linear range between I_p and −log C_{S2} was obtained to be from 1.0×10^{-11} to 1.0×10^{-7} M (inset in Figure 7B), and the detection limit of the biosensor was estimated to be 5.1×10^{-12} M. Obviously, compared to S1/pTSC/GCE, the S1/pTSC/$rCoS_2$/GCE had the wider linear range and the lower detection limit, presenting a superior analytical performance. This further demonstrated that the presence of the $rCoS_2$ on the sensing interface played an important role in enhancing the analytical performance of the biosensor because of its surface area effect and electrocatalytic ability. In addition, the linear range and the detection limit were compared with those obtained on the other biosensors that also use inorganic materials and functional polymer as DNA immobilization platform. The results are displayed in Table 2. From the comparison, it can be seen that

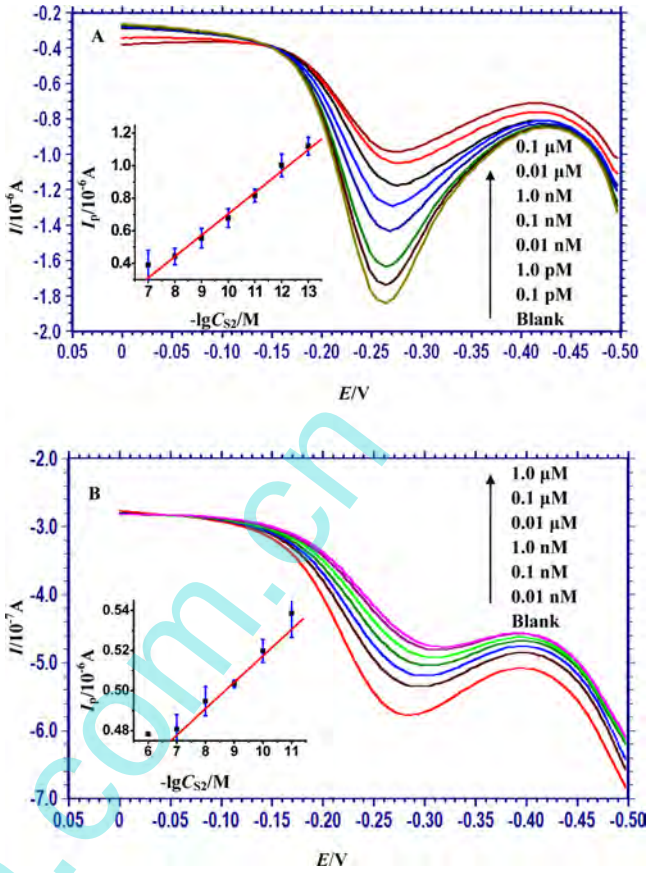

Figure 7. DPVs of MB on S1/pTSC/$rCoS_2$/GCE (A) and S1/pTSC/GCE (B) after hybridization with increasing amount of target DNA (S2). Insets show the calibration curve for I_p versus −lgC_{S2}. The error bars are the relative standard deviation of three independent measurements.

the proposed DNA biosensor exhibited the lowest detection limit and the widest detection range for the target DNA.

3.5. Stability, Reusability, and Reproducibility of DNA Biosensor. The reproducibility of the DNA biosensor was also investigated. Three DNA sensors were fabricated independently under the same conditions and used to detect 1.0×10^{-7}

Table 2. Analytical Performance of DNA Biosensors Designed with Different Inorganic Material or Organic Polymer Composites As Probe Immobilization Matrix[a]

probe immobilization matrix	linear range (M)	detection limit (M)	refs
PABSA/TiO_2 nanosheet	1.0×10^{-11}–1.0×10^{-6}	1.7×10^{-12}	13
nano-SiO_2/PATP	1.0×10^{-11}–1.0×10^{-6}	1.5×10^{-12}	45
Ag_{nano}/PPAA/MWCNTs	9.0×10^{-12}–9.0×10^{-9}	3.2×10^{-12}	46
Au_{nano}-CNT/PAN_{nano}	1.0×10^{-12}–1.0×10^{-6}	5.6×10^{-13}	47
Au_{nano}/poly(L-lysine)	1.0×10^{-13}–1.0×10^{-11}	3.5×10^{-14}	48
pTSC/$rCoS_2$	1.0×10^{-13}–1.0×10^{-7}	1.1×10^{-14}	this work

[a] p-aminobenzenethiol (PATP), poly(m-amino-benzenesulfonic) acid (PABSA), poly(3-(3-pyridyl) acrylic acid) (PPAA), polyaniline nanofiber (PAN_{nano}).

DOI: 10.1021/ie503831k
Ind. Eng. Chem. Res. 2015, 54, 1520−1528

M complementary DNA. The relative standard deviation (RSD) was 3.4%. The regeneration of this DNA biosensor was performed in hot water (90 °C) for 10 min; the biosensor was then cooled rapidly in an ice−salt bath and subsequently rinsed with DDW. The DPV responses of MB at the regenerated electrode and its hybridized electrode were recorded. The two DPV peaks at the two electrodes were approximately the same as those obtained in the initial experiment. Such a regeneration experiment could be performed for at least 5 rounds without losing the hybridization ability. When the DNA biosensor was stored in the refrigerator at 4 °C and then measured after 7 days, no apparent change in signal was observed, indicating that the proposed DNA biosensor had good stability.

4. CONCLUSION

A novel inorganic−organic composite matrix composed of rugby-ball-shaped CoS_2 and poly(2-thiophenesulfonyl chloride) has been developed for DNA immobilization in this work. Electrochemical characterization experiments indicated that the presence of $rCoS_2$ in the composite matrix significantly increased the effective surface area and electrocatalytic capacity of the electrode. Then the synthetic DNA fragments from colitoxin were anchored on the surface of pTSC/$rCoS_2$ through condensation reaction between amino group on DNA and sulfonyl on pTSC. The process was facile and direct and did not require the aid of any other cross-linker used in the conventional method. Because of the high electrocatalytic capacity and large surface area effect of the DNA immobilization platform, the biosensor displayed a wide dynamic range from 1.0×10^{-13} to 1.0×10^{-7} M and a low detection limit of 1.1×10^{-14} M for target DNA. In addition, the biosensor showed high stability, reusability, and reproducibility due to the cocontributions from the steady electropolymerization film of pTSC and the tight sulfamide bond between the probe DNA and pTSC. Therefore, this work illustrates a promising approach for the development of easy and high-performance biosensors.

AUTHOR INFORMATION

Corresponding Author

*E-mail: axiang236@126.com. Tel.: +86-596-2591445. Fax: +86-596-2520035.

Notes

The authors declare no competing financial interest.

ACKNOWLEDGMENTS

The work is supported by the National Natural Science Foundation of China (21275127), Program for New Century Excellent Talents in Fujian Province University (JA12204), the Natural Science Foundation of Zhangzhou (ZZ2012J01), and the key laboratory of urban environment and health, institute of urban environment, Chinese Academy of Sciences (KLUEH201305).

REFERENCES

(1) Luo, C.; Tang, H.; Cheng, W.; Yan, L.; Zhang, D.; Ju, H.; Ding, S. A sensitive electrochemical DNA biosensor for specific detection of Enterobacteriaceae bacteria by Exonuclease III-assisted signal amplification. *Biosens. Bioelectron.* **2013**, *48*, 132−137.

(2) Sun, X. L.; Guan, L.; Shan, X. H.; Zhang, Y. Z.; Li, Z. J. Electrochemical detection of peanut allergen Ara h 1 using a sensitive DNA biosensor based on stem−loop probe. *J. Agric. Food Chem.* **2012**, *60*, 10979−10984.

(3) Nur Topkaya, S.; Aydinlik, S.; Aladag, N.; Ozsoz, M.; Ozkan-Ariksoysal, D. Different DNA immobilization strategies for the interaction of anticancer drug irinotecan with DNA based on electrochemical DNA biosensors. *Comb. Chem. High Throughput Screening* **2010**, *13*, 582−589.

(4) Wang, P. P.; Ni, Y. N.; Kokot, S. A novel dsDNA/polydiphenylamine-4-sulfonic acid electrochemical biosensor for selective detection of the toxic catechol and related DNA damage. *Analyst (Cambridge, U.K.)* **2013**, *138*, 1141−1148.

(5) Wang, X.; Wang, X.; Wang, X.; Chen, F.; Zhu, K.; Xu, Q.; Tang, M. Novel electrochemical biosensor based on functional composite nanofibers for sensitive detection of p53 tumor suppressor gene. *Anal. Chim. Acta* **2013**, *765*, 63−69.

(6) Chen, X.; Hong, C. Y.; Lin, Y. H.; Chen, J. H.; Chen, G. N.; Yang, H. H. Enzyme-free and label-free ultrasensitive electrochemical detection of human immunodeficiency virus DNA in biological samples based on long-range self-assembled DNA nanostructures. *Anal. Chem.* **2012**, *84*, 8277−8283.

(7) Rai, V.; Nyine, Y. T.; Hapuarachchi, H. C.; Yap, H. M.; Ng, L. C.; Toh, C. S. Electrochemically amplified molecular beacon biosensor for ultrasensitive DNA sequence-specific detection of *Legionella* sp. *Biosens. Bioelectron.* **2012**, *32*, 133−140.

(8) Chen, Y.; Wang, Q.; Xu, J.; Xiang, Y.; Yuan, R.; Chai, Y. A new hybrid signal amplification strategy for ultrasensitive electrochemical detection of DNA based on enzyme-assisted target recycling and DNA supersandwich assemblies. *Chem. Commun. (Cambridge, U.K.)* **2013**, *49*, 2052−2054.

(9) Wang, Q.; Ding, Y.; Gao, F.; Jiang, S.; Zhang, B.; Ni, J.; Gao, F. A sensitive DNA biosensor based on a facile sulfamide coupling reaction for capture probe immobilization. *Anal. Chim. Acta* **2013**, *788*, 158−164.

(10) Zheng, D.; Wang, Q.; Gao, F.; Wang, Q.; Qiu, W.; Gao, F. Development of a novel electrochemical DNA biosensor based on elongated hexagonal-pyramid CdS and poly-isonicotinic acid composite film. *Biosens. Bioelectron.* **2014**, *60*, 167−174.

(11) Yang, T.; Li, Q. H.; Meng, L.; Wang, X. H.; Chen, W. W.; Jiao, K. Synchronous electrosynthesis of poly (xanthurenic acid)-reduced graphene oxide nanocomposite for highly sensitive impedimetric detection of DNA. *ACS Appl. Mater. Interfaces* **2013**, *5*, 3495−3499.

(12) Zhang, X.; Gao, F.; Cai, X. L.; Zheng, M. X.; Gao, F.; Jiang, S. L.; Wang, Q. X. Application of graphene-pyrenebutyric acid nanocomposite as probe oligonucleotides immobilization platform in a DNA biosensor. *Mater. Sci. Eng., C* **2013**, *33*, 3851−3857.

(13) Raveh, M.; Liu, L.; Mandler, D. Electrochemical co-deposition of conductive polymer−silica hybrid thin films. *Phys. Chem. Chem. Phys.* **2013**, *15*, 10876−10884.

(14) Justin, P.; Rao, R. G. CoS spheres for high-rate electrochemical capacitive energy storage application. *Int. J. Hydrogen Energy* **2010**, *35*, 9709−9715.

(15) Gu, Y.; Xu, Y.; Wang, Y. Graphene-wrapped CoS nanoparticles for high-capacity lithium-ion storage. *ACS Appl. Mater. Interfaces* **2013**, *5*, 801−806.

(16) Plante, M. P.; Bérubé, E.; Bissonnette, L.; Bergeron, M. G.; Leclerc, M. Polythiophene biosensor for rapid detection of microbial particles in water. *ACS Appl. Mater. Interfaces* **2013**, *5*, 4544−4548.

(17) Goncalves, V. C.; Balogh, D. T. Optical chemical sensors using polythiophene derivatives as active layer for detection of volatile organic compounds. *Sens. Actuators, B* **2012**, *162*, 307−312.

(18) Kaminorz, Y.; Smela, E.; Johansson, T.; Brehmer, L.; Andersson, M. R.; Inganäs, O. Characteristics of polythiophene surface light emitting diodes. *Synth. Met.* **2000**, *113*, 103−114.

(19) Stylianakis, M. M.; Stratakis, E.; Koudoumas, E.; Kymakis, E.; Anastasiadis, S. H. Organic bulk heterojunction photovoltaic devices based on polythiophene−graphene composites. *ACS Appl. Mater. Interfaces* **2012**, *4*, 4864−4870.

DOI: 10.1021/ie503831k
Ind. Eng. Chem. Res. 2015, 54, 1520−1528

(20) Liu, P.; Wu, Y. L.; Pan, H. L.; Ong, B. S.; Zhu, S. P. High-performance polythiophene thin-film transistors processed with environmentally benign solvent. *Macromolecules* **2010**, *43*, 6368−6373.
(21) Liu, M. Q.; Luo, C. H.; Peng, H. Electrochemical DNA sensor based on methylene blue functionalized polythiophene as a hybridization indicator. *Talanta* **2012**, *88*, 216−221.
(22) Charlebois, I.; Gravel, C.; Arrad, N.; Boissinot, M.; Bergeron, M. G.; Leclerc, M. Impact of DNA sequence and oligonucleotide length on a polythiophene-based fluorescent DNA biosensor. *Macromol. Biosci.* **2013**, *13*, 717−722.
(23) Aeiyach, S.; Bazzaoui, E. A.; Lacaze, P. C. Electropolymerization of thiophene on oxidizable metals in organic media. *J. Electroanal. Chem.* **1997**, *434*, 153−162.
(24) Krische, B.; Zagorska, M. Polythiophene synthesis by electropolymerization of thiophene and bithiophene. *Synth. Met.* **1989**, *33*, 257−267.
(25) Abasiyanik, M. F.; Senel, M. Immobilization of glucose oxidase on reagentless ferrocene-containing polythiophene derivative and its glucose sensing application. *J. Electroanal. Chem.* **2010**, *639*, 21−26.
(26) Aysegul, U. DNA hybridization electrochemical biosensor using a functionalized polythiophene. *Talanta* **2009**, *79*, 194−198.
(27) Senel, M.; Dervisevic, M.; Cevik, E. A novel amperometric glucose biosensor based on reconstitution of glucose oxidase on thiophene-3-boronic acid polymer layer. *Curr. Appl. Phys.* **2013**, *13*, 1199−1204.
(28) Cai, H.; Zhu, N.; Jiang, Y.; He, P.; Fang, Y. Cu@Au alloy nanoparticle as oligonucleotides labels for electrochemical stripping detection of DNA hybridization. *Biosens. Bioelectron.* **2003**, *18*, 1311−1319.
(29) Wang, Q.; Zhang, B.; Lin, X.; Weng, W. Hybridization biosensor based on the covalent immobilization of probe DNA on chitosan-mutiwalled carbon nanotubes nanocomposite by using glutaraldehyde as an arm linker. *Sens. Actuators, B* **2011**, *156*, 599−605.
(30) Qiu, B.; Zhao, X.; Xia, D. In situ synthesis of CoS_2/RGO nanocomposites with enhanced electrode performance for lithium-ion batteries. *J. Alloys Compd.* **2013**, *579*, 372−376.
(31) Córdoba, L. F.; Sachtler, W. M.; Montes de Correa, C. NO reduction by CH_4 over Pd/Co-sulfated zirconia catalysts. *Appl. Catal., B* **2005**, *56*, 269−277.
(32) Xu, M.; Zhang, J.; Wang, S.; Guo, X.; Xia, H.; Wang, Y.; Zhang, S.; Huang, W.; Wu, S. Gas sensing properties of SnO_2 hollow spheres/polythiophene inorganic−organic hybrids. *Sens. Actuators, B* **2010**, *146*, 8−13.
(33) Zhou, Y.; Yin, H.; Meng, X.; Xu, Z.; Fu, Y.; Ai, S. Direct electrochemistry of sarcosine oxidase on graphene, chitosan and silver nanoparticles modified glassy carbon electrode and its biosensing for hydrogen peroxide. *Electrochim. Acta* **2012**, *71*, 294−301.
(34) Zhao, D.; Zhang, X.; Feng, L.; Jia, L.; Wang, S. Simultaneous determination of catechol and hydroquinone based on poly (diallyldimethylammonium chloride) functionalized graphene-modified glassy carbon electrode. *Colloids Surf., B* **2009**, *74*, 317−321.
(35) Chakraborty, I.; Malik, P. K.; Moulik, S. P. Preparation and characterisation of CoS_2 nanomaterial in aqueous cationic surfactant medium of cetyltrimethylammonium bromide (CTAB). *J. Nanopart. Res.* **2006**, *8*, 889−897.
(36) Chen, J.; Zhang, J.; Wang, K.; Lin, X.; Huang, L.; Chen, G. Electrochemical biosensor for detection of BCR/ABL fusion gene using locked nucleic acids on 4-aminobenzenesulfonic acid-modified glassy carbon electrode. *Anal. Chem.* **2008**, *80*, 8028−8034.
(37) Prabhakar, N.; Arora, K.; Singh, H.; Malhotra, B. Polyaniline based nucleic acid sensor. *J. Phys. Chem. B* **2008**, *112*, 4808−4816.
(38) Niu, X.; Lan, M.; Zhao, H.; Chen, C. Highly sensitive and selective nonenzymatic detection of glucose using three-dimensional porous nickel nanostructures. *Anal. Chem.* **2013**, *85*, 3561−3569.
(39) Li, F.; Han, X.; Liu, S. Development of an electrochemical DNA biosensor with a high sensitivity of fM by dendritic gold nanostructure modified electrode. *Biosens. Bioelectron.* **2011**, *26*, 2619−2625.
(40) Zhu, N.; Chang, Z.; He, P.; Fang, Y. Electrochemically fabricated polyaniline nanowire-modified electrode for voltammetric detection of DNA hybridization. *Electrochim. Acta* **2006**, *51*, 3758−3762.
(41) Laviron, E. General expression of the linear potential sweep voltammogram in the case of diffusionless electrochemical systems. *J. Electroanal. Chem. Interfacial Electrochem.* **1979**, *101*, 19−28.
(42) Ortiz, M.; Fragoso, A.; Ortiz, P. J.; O'Sullivan, C. K. Elucidation of the mechanism of single-stranded DNA interaction with methylene blue: A spectroscopic approach. *J. Photochem. Photobiol., A* **2011**, *218*, 26−32.
(43) Tani, A.; Thomson, A. J.; Butt, J. N. Methylene blue as an electrochemical discriminator of single-and double-stranded oligonucleotides immobilised on gold substrates. *Analyst (Cambridge, U.K.)* **2001**, *126*, 1756−1759.
(44) Yang, W.; Ozsoz, M.; Hibbert, D. B.; Gooding, J. J. Evidence for the direct interaction between methylene blue and guanine bases using DNA-modified carbon paste electrodes. *Electroanalysis* **2002**, *14*, 1299−1302.
(45) Ma, Y.; Jiao, K.; Yang, T.; Sun, D. Sensitive PAT gene sequence detection by nano-SiO_2/*p*-aminothiophenol self-assembled films DNA electrochemical biosensor based on impedance measurement. *Sens. Actuators, B* **2008**, *131* (56), 5−571.
(46) Zhang, Y.; Zhang, K.; Ma, H. Electrochemical DNA biosensor based on silver nanoparticles/poly(3-(3-pyridyl) acrylic acid)/carbon nanotubes modified electrode. *Anal. Biochem.* **2009**, *387*, 13−19.
(47) Zhou, N.; Yang, T.; Jiang, C.; Du, M.; Jiao, K. Highly sensitive electrochemical impedance spectroscopic detection of DNA hybridization based on Aunano-CNT/PANnano films. *Talanta* **2009**, *77*, 1021−1026.
(48) Wang, J.; Zhang, S.; Zhang, Y. Fabrication of chronocoulometric DNA sensor based on gold nanoparticles/poly(L-lysine) modified glassy carbon electrode. *Anal. Biochem.* **2010**, *396*, 304−309.

DOI: 10.1021/ie503831k
Ind. Eng. Chem. Res. 2015, 54, 1520−1528